# Defense Technical Information Center Compilation Part Notice

# ADP010744

TITLE: Molecular Diagnostics for the Study of Hypersonic Flows



## This paper is part of the following report:

TITLE: Measurement Techniques for High Enthalpy and Plasma Flows [Techniques de mesure pour les ecoulements de plasma et les ecoulements a haute enthalpie]

To order the complete compilation report, use: ADA390586



The following component part numbers comprise the compilation report:

ADP010736 thru ADP010751

# Molecular Diagnostics for the Study of Hypersonic Flows

**F. Grisch**
Office National d'Etudes et de Recherches Aérospatiales
Département Mesures Physiques
29, Avenue de la DivisionLeclerc
92320 Châtillon Cedex
France

## Summary

New laser-based diagnostic techniques offer considerable promise for measurements in hypersonic flows. In this paper , we overview optical techniques such as Rayleigh and Raman scattering, laser-induced fluorescence, electron beam fluorescence, coherent anti-Stokes Raman scattering and diode laser absorption. These methods have unique capabilities for nonintrusive measurements of flowfield parameters such as temperature, density, species concentration and velocity. The applicability of these techniques for the study of hypersonic flows is also presented.

## Introduction and Scope

The interest in reentry of space vehicles, in high speed transportation, and in single stage-to-orbit concepts continues to stimulate the research into supersonic and hypersonic aerodynamics. This research is conducted in facilities that basically simulate flight at high altitude and high velocity.

Short-duration test facilities such as the hypersonic shock tunnel, however, have afforded a means for extending research study capabilities into the high velocity flight regime. The development of ground test facilities to simulate the flow about hypersonic vehicles is nevertheless very challenging because of the high total enthalpies required. The stagnation enthalpies encountered in flight at hypersonic velocities result in flowfield temperatures high enough to dissociate and even ionize the chemical species in air. The reservoir state in a short duration test facility, which then undergoes expansion to high velocity is, of course, at comparable enthalpies to the flight case. The test gas in reservoir is therefore also dissociated and ionized. In the subsequent expansion to hypersonic speeds, the flow can depart from thermal and chemical equilibrium.

It is in the test flow environments that perfect gas reciprocity is lost since, at comparable velocities, the freestream in the high enthalpy facility test section differs from that existing for flight in the atmosphere. The static pressures and temperatures (and hence the Mach numbers) differ and the composition of the air contains oxygen atoms and nitric oxide, in addition to the $O_2$ and $N_2$ molecules. At higher enthalpies, nitrogen is also appreciably dissociated and ionized species begin to appear in significant concentration. The ionization introduces plasma properties into the flow environment which can leads to additional interaction phenomena associated with the presence of a free electron concentration in the flowfield. The effect of the nonequilibrium free stream composition on flowfield measurements around a test model must then be understood in order to relate to the flight case. Computer codes exist, of course, for the prediction of nonequilibrium flow expansions, and for flows about high velocity vehicles. The important questions are the followings: Is the chemistry fully specified? Are the reactions reliable?

In high enthalpy facility operations, therefore, it is necessary that consideration must be given to the diagnostic methods and techniques available for independent measurement of species compositions. A description of such complementary techniques will comprise the substance of the lecture discussions. The methods to be discussed have all appeared, in various forms, in the literature on research studies covering a range of different flow environments and gas mixtures.

With the advent of laser light sources, light scattering spectroscopic diagnostic techniques are assuming an ever-increasing role in a broad spectrum of physical investigations. There is a large variety of diagnostic processes potentially applicable to the remote, nonintrusive, point and imaging probing of hypersonic flows. The subject of hypersonic diagnostics has received a great deal of attention in the past few years. A review of the techniques for hypersonics that were available a

*Paper presented at the RTO AVT Course on "Measurement Techniques for High Enthalpy and Plasma Flows", held in Rhode-Saint-Genèse, Belgium, 25-29 October 1999, and published in RTO EN-8.*

few years ago can be found in Ref. 1. A special issue of the AIAA Journal has been devoted to advanced measurements technologies [2].

Attention will be directed ultimately only to those laser techniques which can permit the determination of local species concentration, temperature and velocity measurements. In the first part of this review, we present potential optical techniques such as the Rayleigh scattering, the spontaneous Raman spectroscopy (SRS), the coherent anti-Stokes Raman spectroscopy (CARS) and the laser induced fluorescence (LIF) which allows points measurements. These techniques provide good spatial resolution, either via the use of the configuration of the laser beams (CARS) or by monitoring a small elemental length of the laser beam (SRS, LIF,...). We also present the electron beam fluorescence (EBF), which is also a suitable technique to determine the number density and velocity.

Other optical techniques to be discussed involve emission or absorption phenomena which exploit the idea that air species in real-gas flows are optically active and allow emission or absorption spectroscopic techniques to be used. These latter are integrated line of sight measurements which are appropriate, for instance, for the characterization of the quasi one-dimensional flows in a nozzle expansion. In particular, diode laser absorption spectroscopy has a potential for great accuracy in the acquisition of the translational temperature and velocity.

From this exhaustive list, three techniques, which are mainly used at ONERA for the study of high-enthalpy flows will be selected for a detailed evaluation including: Coherent anti-Stokes Raman Spectroscopy, electron beam fluorescence and Diode laser absorption spectroscopy.

## Review of potential hypersonic diagnostic techniques

Measurements are primarily performed by using laser scattering off the molecules or particles seeded into the flow. They can be implemented using their incoherent scattering of a laser beam or coherent, nonlinear optical arrangements; the molecules can also be excited by electrons beams of several kiloelectron volts, which can induce fluorescence in the visible, ultraviolet and X ray regions.

### *Incoherent Scattering*

Incoherent scattering is observed by illuminating the gas with a focused laser beam. The light scattered at right angles by the gas molecules is collected by a lens, spectrally analyzed using a spectrograph, and detected by means of PM tubes or detector arrays. Three sorts of scattering processes in molecules are commonly recognized and schematically depicted in the energy-level diagrams in Figure 1. Commercial pulsed lasers can be employed, giving a typical time resolution of 10 ns, which is suitable for short-duration facilities. The energy per pulse needed is in the range 10-100 mJ. Continuous wave lasers also can be used for steady state flows, and the spatial resolution is typically 0.1-1 $mm^3$.

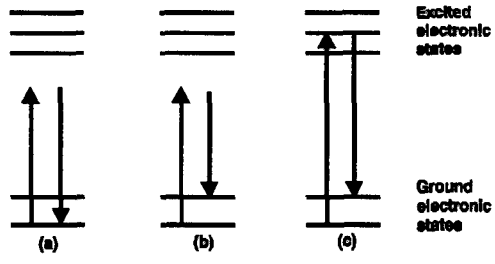


*Figure 1* Energy level diagram for Rayleigh (a), Raman (b), and fluorescence (c) scattering.

#### *Rayleigh Scattering*

The elastic scattering of light quanta from molecules is termed Rayleigh scattering and is the phenomenon giving rise to the blue appearance of the sky. Because the scattering process is elastic, the photons are scattered in all directions and have the same energy as the laser photons. the scattered light is unshifted in frequency and, hence, not specific to the molecule causing the scattering. Thus the technique can be used for total density measurements but not for individual species concentrations. From a practical viewpoint, Rayleigh scattering is a weak process that requires total absence of stray light at or near the laser wavelength. Also, the laser should not impact any solid surface near the volume under probe to avoid strong interference. Particles suspended in the flow also cause Mie scattering (see below) that constitutes another form of interference. This problem actually limits the sensitivity of the method to densities of the order $10^{-1}$-$10^{-2}$ normal at best. Its potential use is thus restricted to classical subsonic and low supersonic tunnels. Proximity of a wall is also a major source of interference because the laser light scattered off the surface is many orders of magnitude stronger than that from the molecules. Rayleigh scattering is thus proscribed in boundary layers studies. Filtered Rayleigh scattering can solve that problem [3].

*Mie Scattering*

Elastic scattering of light quanta from particulate matter is termed Mie scattering. Mie scattering designates the signal scattered by particles with sizes comparable to or larger than the wavelength of the illuminating laser (0.4-0.6 nm, typically). It is a close parent of Rayleigh scattering. It is not dependent on molecular number density or temperature and, hence, cannot be used to provide such information. It is the basic effect underlying the Laser Doppler Velocimetry (LDV) [4]. While LDV works remarkably well in subsonic and low supersonic flows, it has met with mixed success in hypersonic, because the low density is too low to carry the particles, especially through shocks. An interesting assessment is found in Ref.1. It can be a very strong process depending on particle number density and particle size, and is a potential source of interference in high enthalpy flows.

*Spontaneous Raman Scattering*

Raman scattering is the inelastic scattering of light from molecules as illustrated in Fig.1 and is termed rotational, vibrational or electronic depending on the nature change which occurs in the molecule. The process is essentially instantaneous occurring within a time of $10^{-12}$ s or less. The molecule may either become excited or deexcited depending on its original state prior to the interaction. Due to the quantization of the molecular energy states, the Raman spectrum is located at fixed frequency separations from the laser line characteristic of the molecule from which the scattering emanates. This property is extremely interesting, because it offers chemical selectivity, since the frequency difference, which is proportional to the vibrational quanta, differs from molecule to molecule. Spectroscopy of the scattered light thus reveals the presence of the various chemicals and allows concentration measurements. It also offers temperature measurement capacity: the energy of the vibrational quantum slightly depends on the rotational state of the molecule. Each rotational state thus gives a specific line, which is separable from its neighbors under high spectroscopic resolution. The states being populated according to Boltzmann's law, spectral analysis yields the rotational temperature; the latter is generally equal to the static temperature of the gas. Measurement accuracy is of the order of 50-100 K if the signal-to-noise ratio is good. Even better performance seems attainable under special conditions using a variant called rotational Raman scattering.

Unfortunately, Raman scattering is weaker than Rayleigh scattering, typically by a factor of 100-1000. Its use, in spite of its other attractive characteristics, is thus restricted to aerodynamic flows above or close to normal density, and to weakly luminous flames. Its effective detection sensitivity with state-of-the-art lasers and detection optics is in the range $10^{15}$-$10^{16}$ molecules $cm^{-3}$ for a spatial resolution set at 1 $mm^3$. Thus, it has a little future in hypersonics with today's lasers and detectors unless densities as high as at least $10^{-1}$ normal are achieved in the free stream, and stray light and flow luminosity are kept very low. Some applications of Raman scattering to aerodynamics flows can be found in [5, 6].

*Fluorescence Scattering*

Fluorescence is the emission of light from an atom or molecule following promotion to an excited state by various means: heating, chemical reaction (chemiluminescence), electron bombardment, or absorption. Here only the two last means will be considered. The precise definition of fluorescence requires that emission occur between electronic energy states of the same multiplicity, i.e. the same electronic spin states. Emission between states of different electronic spin is called phosphorescence. In general, fluorescence lifetimes are between $10^{-10}$ and $10^{-5}$ s, much shorter than the phosphorescent lifetimes of $10^{-4}$ s to seconds. The light emission may be shifted in wavelength from the incident light (fluorescence) or occur at the same wavelength (resonance fluorescence). In general, it is desirable to examine shifted emission to avoid potential from particles (Mie scattering) or spurious laser scattering.

Fluorescence is of diagnostic interest since it combines the species selectivity of Raman scattering with far stronger signal intensities. It is closely related to Raman, but with the exciting laser tuned onto resonance with the one-photon absorption lines of the molecule of interest. This trick enhances the scattering cross section – and therefore the signal strength – by many orders of magnitude and makes it possible to detect parts-per-million-level traces in flames as the OH radical and the NO pollutant. Detection sensitivities lie in the range $10^{10}$-$10^{12}$ $cm^{-3}$.

The principles of LIF are well-known (see refs. 7-8 and articles cited herein for an up-to-date review) and need not to be repeated in detail here. In brief, a laser source is tuned to excite a specific electronic absorption transition in the species of interest. Following the absorption process, collisional redistribution in the electronically excited state may occur prior to either collisional quenching or radiative de-excitation (fluorescence) of the molecule back to a lower electronic state. The emission, which occurs over a range of wavelengths, is usually collected at right angles

and filtered spectrally at the photodetector. For a given species, the variables in the LIF process are the transition pumped, the detection spectral bandpass, the spectral intensity of the laser, and, in the case of narrow linewidth laser, the location of excitation within the absorption line profile. LIF may be thought of as potentially with the intersection of the illumination and collection beam paths controlling the spatial resolution of the measurement. In the case of sheet beam illumination and detection with an array detector, the size of the detector pixels and the magnification of the collection optics controls the size of the measurement volume at each image "point" [9].

The governing equation of the LIF signal, S, is based on a simple two-level model with weak (unsaturated) excitation, for a single detector pixel, is [10-11]

$$S = CEVN_s BF_{vj}(T)[A/(A+Q)]$$

Here, C is a group of constants specific to the experimental set-up. E is the laser energy per pulse per unit area per unit frequency, V is the measurement volume for the detector element, $N_S$ is the number density of the absorbing species, $F_{vj}$ is the population fraction for the pumped state, B is the Einstein coefficient for absorption, and A is the appropriate (for the transitions monitored) Einstein coefficient for spontaneous emission. The parameter Q represents the sum rate of all other transfer processes which eliminate into the detection bandwidth. In the most common case, these processes are: dissociation, energy transfer to other internal energy states within the same molecule, and chemical reaction. These processes competitive with fluorescence, termed quenching processes, reduce the signal strength which can be obtained and complicate interpretation of the data. In principle, if all the quenching species densities are known, and if all of the appropriate quenching rate is available, analytical quenching corrections to the data would be possible [12, 13].

LIF was at first used for point measurements, particularly in flames and in supersonic, low pressure streams (for mixing studies using traces of iodine gas as a seeder). For the past 5-10 years, however, it has primarily been employed for flame and flowfield imaging (see below), thanks to the introduction of intensified two-dimensional charge-coupled device (CCD) detector arrays. Several applications to hypersonics are compiled in Ref. 1. Recent work has focused on concentration measurements of copper [14] and oxygen atoms [15-16]. By scanning the absorption lines with their tunable lasers, these authors were also able to detect the Doppler shift resulting from the flow motion and to deduce the flow velocity with an accuracy on the order of 10-15 %.

A good application of such work is shown in the following example which illustrates the capabilities of this technique to study high enthalpy flows [17]. The flowfield of the high enthalpy facility L2K of the Deutsche Forshungsanstalt für Luft and Raumfahrt (DLR) have been explored using the LIF technique in order to characterize the conditions in the test section free stream flow and also to probe the shock layer induced by a model placed in the flow. The arc heated facility, which is mainly used for testing thermal protection materials, offers a wide choice of flow conditions to simulate the stagnation conditions during shuttle re-entry. The L2K facility can be operated during several hours without interruption. It uses two hollow copper electrodes and is powered by a direct current power supply. The high enthalpy gas flows through a small settling chamber then through a conical nozzle toward a vacuum chamber. The mass flow rate is 50 g/s. The total enthalpy delivered to the gases is 6.7 MJ/Kg and the stagnation pressure and temperature are 1.3 $10^5$ Pa and 3910 K respectively. The flow field in this facility is dominated by nonequilibrium phenomena.

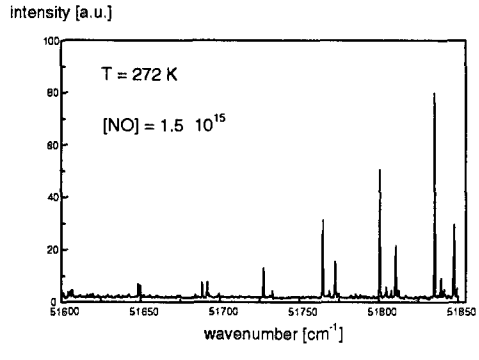


***Figure 2*** Excitation spectrum of NO recorded in the free stream at the LBK facility.

NO has been used as a natural tracer for the LIF experiments. A tunable excimer laser (lambda Physics LPX 150) is operated with ArF to generate light pulses with a duration of 20 ns and a power of up to 240 mJ at the wavelengths of NO transitions in the 192.8 nm–193.8 nm spectral range. Because of the L2K continuous flow, characterization of the free stream flow has been made by recording the excitation spectrum of NO in the flow. For instance, a typical free stream excitation spectrum is shown in Fig 2. The analysis of the line intensities allows the determination of the rotational temperature. The absolute number

density of NO can be also deduced from the comparison of the fluorescence signals with those measured in a calibration experiment where all the physical parameters are known.

Two-dimensional laser induced fluorescence images of NO upstream of the model are also recorded by tuning the laser to a NO transition (excitation frequency of 51625 $cm^{-1}$). Figure 3 shows clearly the shock shape with a shock stand off of 13-14 mm at the model axis. The increase of the NO fluorescence signal behind the shock front is related to the increase of the number density and to the temperature elevation. Due to quenching effects, the fluorescence intensity decreases in region close to the model.

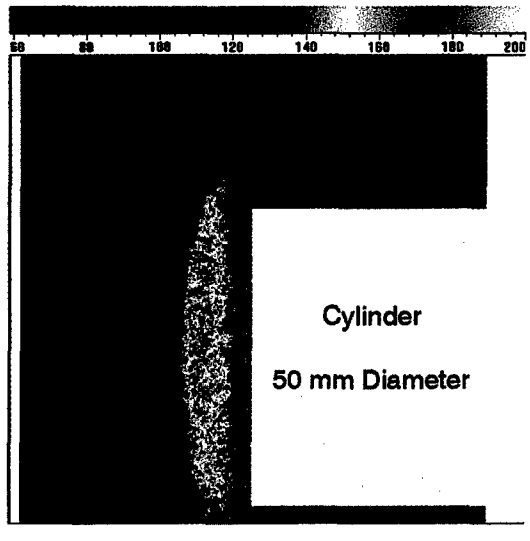


***Figure 3*** Two-dimensional LIF image of NO recorded upstream of the model at the LBK facility

***Electron beam Fluorescence***

Electron beam fluorescence (EBF) bears some resemblance to LIF excepted that the laser beam is replaced by a high energy electron beam. Electron guns such as those employed in electron microscopy are used, but even more powerful sources like pseudo-sparks are sometimes utilized. The high energy electrons induce broadband excitations onto the molecules under probe and eventually ionize them. For nitrogen at $10^{-4}$ normal density, the main process is

$$N_2 + e_p^- \rightarrow N_2^{+*} + e_p^- + e_s^-$$

Where $e^-_p$ is a primary electron (from the electron beam) and $e^-_s$ a secondary electron of an energy of a few electron volts emitted during the formation of the $N_2^+$ ion. This ion, which is excited by the collision on one of its vibronic states, denoted by the * symbol, promptly loses its energy via emission of a photon,

$$N_2^{+*} \rightarrow N_2^+ + h\nu$$

in the near ultraviolet. The luminescence is interesting because its intensity is proportional to the $N_2$ number density and its spectral content reveals the original population distribution on the quantum states of the $N_2$, allowing temperature measurements to be performed. The secondary electrons remain confined in the immediate vicinity of the ions by the space charge and continue to have low-energy collisions with them; these collisions reexcite them and maintain a luminescence by the processes

$$N_2^+ + e_s^- \rightarrow N_2^{+*} + e_s^-$$

$$N_2^{+*} \rightarrow N_2^+ + h\nu$$

This causes the luminescence to persist several microseconds or tens of microseconds after the high-energy electron beam has been turned off. This phenomena can be exploited for free stream velocity measurements by flow tagging, followed by time-of-flight detection [18]. EBF also measures rotational and vibrational temperatures by dispersing the spectrum of the emitted fluorescence.

Typical applications of EBF can be found in ref. 1. Both point measurements and imaging (see below) are used. The spatial resolution is of the order of 1 $mm^3$; it is usually a little worse than in the laser scattering techniques. Recently, encouraging results were reported using a pseudo-spark mounted on a model [19]. However, EBF suffers from a difficulty associated with quenching:

$$N_2^{+*} + N_2 \rightarrow N_2^+ + N_2$$

Quenching reduced the fluorescence yield and interferes with the concentration measurements at densities above a few $10^{-4}$ normal. Detection of the X-ray emission, which results from a Brehmstrahlung process and suffers no quenching, offers an interesting alternative [20].

EBF has so far been used primarily in low and medium enthalpy facilities for imaging. Illumination is achieved by rastering the continuous-wave beam emitted by the electron gun, giving a triangular field. Mohamed et al. have done interesting studies using this method on shock-shock interaction configurations between a flat plate and a cylinder [18]. In spite of the quality of such images, work at high enthalpy facilities is impaired by the weakness of the scattering and the strength of the stray light. Higher-current electron

beams are thus required. Recently, a new electron-beam source based on a pseudospark electron gun and capable of delivering a thin-pulsed sheet 45 cm in length has been developed at Onera. This source shows great promise for future work in high-enthalpy facilities. However, the main constraint is that flows should not exceed densities of $10^{-3}$ normal to avoid excessive electron-beam blowup.

The pseudospark technology consists of two electrodes in the form of coaxial disks, each with a central hole, separated by a gap of a few millimeters. (Fig 4). The upper disk forms the cathode, whereas the lower one acts as the anode. Injection of $10^{9}$-$10^{10}$ electrons to the back of the cathode induces the electrical breakdown of the gap between the two electrodes. The standing voltage that can exceed 60 kV for a single-stage apparatus then, typically, collapses to zero in 20-50 ns. This is simultaneously accompanied by emission of a very bright pinched electron beam along the axis of the disks. The maximum current is then 300-1000 A, the mean section is in the square millimeter range, and the electron energy is related to the instantaneous voltage between the electrodes. The fast electrons exit the anode disk orifice and can propagate for a few tens of centimeters in a low-pressure medium. In practice, the pseudospark, which operates in a same gas as the flow, is provided with its proper gas-pressure control device and communicates with the wind tunnel through a reduced hole of 0.3 mm diameter. This allows one both to achieve a narrower electron beam for the
gas ionization trace and to maintain a low pressure inside the pseudospark.

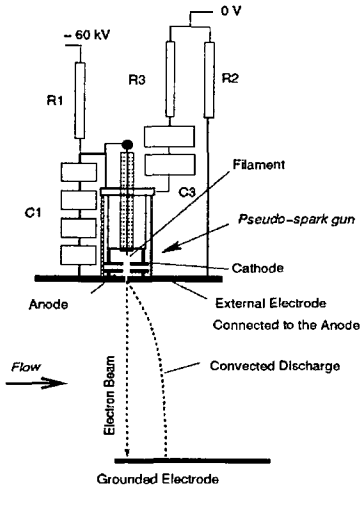


***Figure 4*** Schematic diagram of the pseudo-spark electron gun for velocity measurement

A solution avoiding the important problem of the ionization of the gas leading to the production of the conductive plasma of ions and secondary electrons has been elaborated to maintain the electron beam elsewhere in the wind tunnel. The proposed strategy was to use simultaneously the fast electron emission by the pseudospark, together with its high-voltage breakdown capability, to sustain across the plasma column a supplementary discharge current of much longer duration than the pulsed-electron beam. This induces an intense fluorescence that persists for some microseconds, as long as an electrical current of a few amperes feeds the conductive trace. During this time, the column is convected and deformed by the flow following the velocity profile that is present.

Using an intensified CCD camera, the column of the gas can be photographed after some delay, showing its displacement. One can then visualize the velocity field along a line, over a length of about 25 cm.

This approach has been tested successfully recently at the F4 high-enthalpy wind tunnel [21]. Figure 5 shows the image acquired 90 ms after the onset of the shot, during a typical run at stagnation conditions, 215 bars and 7.8 MJ/kg. The plasma column convected by the flow after 5 μs can be seen at the upper part of the image. The top of the column, which lies in the boundary layer, is bent, showing the velocity profile. Fig 6 shows the velocity profile deduced by the best fit of the image of Fig. 6. The highest velocity, i. e., 4100 m/s (± 5%) at 150 mm from the external boundary of the stream, correlates well with the theory.

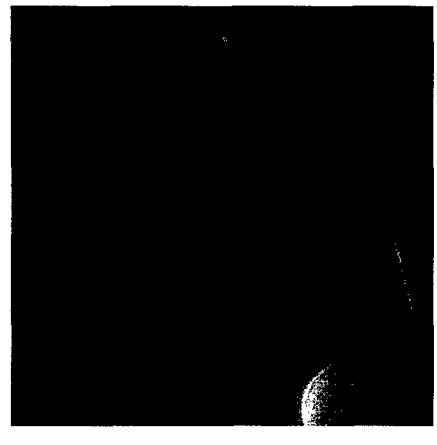

***Figure 5*** Typical F4 run, flow at 90 ms, convection imaged 5 μs after beam emission.

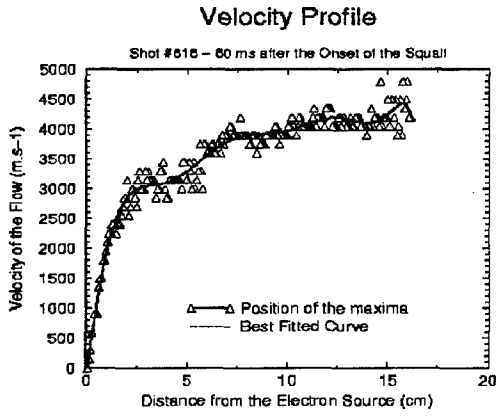


***Figure 6*** Velocity profile at 90 ms for run of Fig.5.

## *Coherent scattering*

***Coherent anti-Stokes Raman Scattering***

The possibility to carry out concentration and temperature measurements by Raman spectroscopy was proved since the seventies. A non linear coherent signal optical process was proposed to solve analysis problems which remain inaccessible using incoherent scattering. This technique, named Coherent anti-Stokes Raman spectroscopy, was observed initially in aromatic liquids in 1965 by Maker and Terhune [22]. The CARS process involves the mixing of four coherent waves, three of them are incident and the fourth one is created in the medium under study. At the beginning, CARS was used for spectroscopic purposes. The idea to employ it to carry out non intrusive analysis in reactive gaseous mixtures was born at ONERA shortly after the seventies.

***a) Principle***

The interaction of light with matter is represented by the classical Maxwell's equations. When the bulk material has no free charges and no magnetization, we obtain (in Gaussian units):

$$\nabla\times(\nabla\times\vec{E}(\vec{r},t))+\frac{1}{c^2}\frac{\partial}{\partial t^2}\vec{E}(\vec{r},t)=-\frac{4\pi}{c^2}\vec{P}(\vec{r},t)$$

Where E(r,t) is the total electric field of the incident waves, c is the speed of light, and P(r,t) the electronic polarization vector. With weak incident electric fields, P responds linearly in terms of E. With more intense fields, P is written in terms of a power series in the field amplitudes:

$$\vec{P}(\vec{r},t)=\vec{P}^{(1)}(\vec{r},t)+\vec{P}^{(2)}(\vec{r},t)+\vec{P}^{(3)}(\vec{r},t)+...$$

Using the following expression for the incident electric field E(r,t) as a function of monochromatic planes waves of frequency $\omega_i$ and of wave vectors $k_i$, the spectral components of the polarization can be written like:

$$\vec{P}^{(n)}(\vec{r},\omega_q)=\left(\frac{1}{2}\right)^{n-1}\chi^{(n)}(-\omega_q,\omega_i,\omega_j,\omega_k)\,\vec{E}(\vec{r},\omega_i)\vec{E}(\vec{r},\omega_j)\vec{E}(\vec{r},\omega_k)$$

with $\omega_q=\Sigma\omega_i$

$\chi^{(1)}$ is the linear susceptibility. This term accounts for the classical phenomena like absorption and refraction. $\chi^{(2)}$ is the second-order susceptibility. This latter vanish in isotropic media and centrosymmetric crystals. In isotropic media, the first non-linear term is $\chi^{(3)}$. This term is responsible for CARS. CARS is observed when three waves with frequencies $\omega_1$ and $\omega_2$ pass through a gas. Incident laser beams at frequencies $\omega_1$ and $\omega_2$ (often termed the pump and the Stokes beams respectively) interact through the third order non linear susceptibility $\chi^{(3)}$ to generate a polarization field which produces coherent radiation at frequency $\omega_3=2\omega_1-\omega_2$. When the frequency difference $(\omega_1-\omega_2)$ is close to the Raman-active vibrational frequency $(\omega_P)$ of a molecular species of the gas, the magnitude of the radiation at $\omega_3$ become very large. Large enough, for instance, that with typical pulsed experimental arrangements, the CARS signal from room air on $N_2$ is visible.

CARS offers very promising potential for the diagnostic probing of hypersonic flows. First, in contrast to spontaneous Raman phenomena, CARS is fairly strong process leading to signal levels typically several orders of magnitude larger than those from Raman scattering. Second, The CARS signals are coherent. Consequently, all of the CARS signal can be collected. Contrast this with the situation pertaining in the incoherent processes where photons are scattered over $4\pi$ steradian and are collected only over a limited solid angle $\Omega$. Furthermore, since the CARS signal can be collected in an small solid angle, discrimination against interference signals like background luminosity, florescence, ... is greatly facilitated. Thus, CARS is expected to produce signal to noise ratio improvements of many orders of magnitude over spontaneous Raman scattering.

The expression of the intensity of the CARS signal at the $\omega_3$ frequency is given by:

$$I_3 = 1.910^{-25}\omega_3^2\left|\chi^{(3)}(-\omega_3,\omega_1,\omega_1,-\omega_2)\right|^2 I_1^2 I_2 z^2$$

where $I_1$and $I_2$ are the beam intensities ($W.cm^{-2}$) at frequency $\omega_1$ and $\omega_2$ respectively and z is the probe length. When the incident beams are focused at the same point, the CARS signal is created mainly in the focal zone. The CARS power depends on those of the incident beams by

$$P_3 = 2.210^{-47}\omega_3^4\left|\chi^{(3)}(-\omega_3,\omega_1,\omega_1,-\omega_2)\right|^2 P_1^2 P_2$$

The expression is obtained assuming that the beams have the same diameter and that their divergence is limited by diffraction. It is independent of the focal strength of the lenses and of the beam diameter. We note also that the signal is proportional to $P_1^2P_2$ which explains the use of high power pulsed lasers.

The susceptibility can be written in terms of a resonant and non-resonant part

$$\chi = \chi_r + \chi_{nr}$$

$\chi^{nr}$ is the contribution from electrons and remote resonances. The resonant susceptibility associated with a homogeneously broadened Raman transition, j is given by

$$\chi_r = \frac{N}{\hbar}\sum_{if}(\omega_{if} - \omega_1 + \omega_2 - \Gamma_{if})^{-1} \times (\rho_{ii}^{(0)} - \rho_{ff}^{(0)}) \times \alpha_{if}^2$$

The subscripts i and f refers to initial and final states respectively. Purely collisional damping is assumed in the eqn., where $\Gamma_{if}$ is the half width and f of the collisional Raman linewidth. Note that the populations appears as a difference between the initial states and the final states. $\alpha_{if}$ is the polarizability matrix element of a specific transition and is related to the well-known Raman cross section by

$$\alpha_{if} = \left(\frac{d\sigma}{d\Omega}\right)_{if}^{1/2}\left(\frac{c}{\omega_2}\right)^2$$

For efficient CARS signal generation, the incident pump and Stokes laser beams must be combined in order to fulfil the phase matching condition

$$\vec{k}_3 = \vec{k}_1 + \vec{k}_1 - \vec{k}_2$$

where $\mathbf{k}_i$ denotes the wave factor at frequency $\omega_i$. This condition stipulates that the anti-Stokes field created at any location by the two laser beams will be phased properly with the anti-Stokes wave coming at upstream positions. The spatial resolution is of the order of 1 cm if one uses collinear beams at the diffraction limit which are focused at the same point of interest under a f–number of 50. For some applications, particularly in turbulent flows, this is insufficient. A better resolution can be obtained with a crossed-beam geometry called BOXCARS [23]. In this configuration, an additional beam of frequency $\omega_1$ is focused at the same point, thus generating a new signal beam in its direction. The latter is generated from the volume common to all the laser beams. The spatial resolution obtained is then of the order of several mm.

All the CARS experiments aim at recording the variations of $P_3$ versus the frequency difference ($\omega_1$-$\omega_2$). The CARS spectrum allows both the chemical and temperature analysis of the gas mixture:

- The spectral positions of the lines or bands are characteristic of the molecular species;
- The line strengths permit the measurement of the molecular densities;
- The population distributions on the diverse quantum states yield the temperature.

Several methods are possible to record CARS spectra. The first one, called scanning CARS, uses a monochromatic laser and a narrow band tunable laser. The spectra are recorded step by step by scanning ($\omega_1$-$\omega_2$), the fixed frequency laser being usually the $\omega_1$ laser. Scanning CARS gives an excellent spectral resolution and a good sensitivity of the order of $10^{14}$ $cm^{-3}$ but, because several minutes are often requested for data recording, only stable or reproducible media can be studied. The second method, called broadband CARS, is well suited to study fluctuating or transient phenomena. It requires a monochromatic laser and a laser covering a wide range of frequencies. The entirety of the CARS spectrum is generated during a single shot laser. The laser energy being now spread over a wide spectral domain, the CARS signal intensity is reduced by several orders of magnitude. The detection limit increases to $10^{17}$ $cm^{-3}$. The third technique, called the dual-line CARS is used to study short-duration low density phenomena., when neither broadband CARS or scanning CARS can be used. It requires a monochromatic laser and two tunable narrow band lasers tuned so that ($\omega_1$-$\omega_2$) and ($\omega_1$-$\omega'_2$) are in resonance with two Raman frequencies of the molecule. Spectra are no longer recorded but the temperature is obtained from the ratio of the two CARS intensities and the density from the line strengths.

*b) experimental setup*

CARS set-up are made up of an emission part and of a reception part separated by the measuring and reference channels. We will describe successively the emission block, a typical arrangement of the measuring and reference channels, and finally the detection system. This later differs according to the type of spectroscopy which is implemented. The instrument developed at ONERA has been conceived to be reliable, transportable and versatile. It allows the three CARS techniques. All the optics, laser sources and mixing optics, are mounted on a transportable table. The main element of the set-up is the Nd:YAG laser chain. The frequency doubled Nd:YAG laser is operated in single longitudinal and transverse mode. This property is felt to be quite important for CARS in the gas phase. A pockels cell is used to trigger the Nd:YAG oscillator. Because there is then no way to maintain the less efficient mode below the threshold, the single mode operation is forced by seeding the oscillator with a CW single mode diode-pumped micro Nd:YAG laser. With one amplifier and a KDP-type 2 frequency doubler, the YAG chain delivers 400 mJ at 532 nm in 11 ns pulses. Using a second KDP crystal like above, gives 70 mJ at 532 nm. This beam is used to pump a dye laser oscillator.

For scanning CARS experiments, the dye laser chain is composed of a dye laser and one amplifier. The oscillator comprises an uncoated wedged output mirror, a 2100 groves/mm grazing incidence grating, a four prism expander and a flat rotating back mirror. The linewidth is 0.07 $cm^{-1}$ (FWHM). The tuning is driven by steeping mirror which allows both a continuous sweep from 500 to 800 nm in coarse steps of 0.07 $cm^{-1}$, and limited sweeps of 6 nm around the coarse drive setting in fine steps of 0.007 $cm^{-1}$. After the amplifier cell, pumped by 1/3 of the main 532 nm beam, the dye chain energy ranges between 1 and 10 mJ depending on the dye and the pump energy.

For broadband CARS experiments, the dye laser chain is also composed of a dye laser and one amplifier. The oscillator is formed by a 100 % back mirror and an uncoated wedged output mirror. A 3 µm-thick Fabry-Perot etalon is used for the tuning. The oscillator is pumped by the second part of the 532 nm generated by the second KDP. The laser linewidth is of the order of 100 $cm^{-1}$. After the amplifier cell, pumped by 1/3 of the main 532 nm beam, the dye chain energy is 5 mJ.

For dual line CARS, both dye lasers are used simultaneously. The linewidth of the broadband laser is narrowed by an interference filter and two intracavity Fabry-Perot etalons. They are 0.1 mm and 1 mm thick respectively. The linewidth is then 0.2 $cm^{-1}$.

Prior leaving the CARS table, the beams are expanded to 6-7 mm by means of telescopes. The Nd:YAG beam passes through a tilted parallel plate which splits the beam into two parallel beams of equal energy. A simple translation of the plate transmits the collinear and BOXCAR arrangements. $\lambda/2$ and $\lambda/4$ wave plates can also be inserted for proper background cancellation at the signal probe volume. Finally, a dichroic mirror is used to align the $\omega_1$ beams along with the $\omega_2$ beam.

It is well known that CARS suffer large shot to shot fluctuations, larger than those due to Poisson statistics. CARS signals usually vary between 1 and 3 successive laser shots which makes it difficult to use CARS without care. The origin of these fluctuations are two fold, apart from those given by the analyzed media:

- the directions and the aberrations of the laser beams vary slightly; this modifies the phase and intensity distribution within the probe volume and consequently changes the signal intensity.
- the mode frequencies and mode amplitudes of the multimode dye lasers are random. The modes excite more or less resonantly the Raman lines. This constitutes the main source of fluctuations when the Raman linewidth is smaller than the free spectral range between the modes as it is encountered in low density media.

The solution, now currently used, consists in dividing the measuring signals by a reference CARS signal measured simultaneously. The optical arrangement of the referencing and measuring channels depends on the experiment. Referencing signal is usually created in a cell filled with one atmosphere of a non resonant gas like Argon. For dual-line CARS, the rare gas referencing is replaced by referencing in the gas analyzed in the measuring channel in order to take into account more precisely the effects of the mode structure of the dye laser.

In scanning CARS, the anti-Stokes signals are filtered by means of compact double monochromators, preceded by dichroic filters to prevent breakdown of the monochromator slits and detected by PM tubes. The latter are mounted in the same rack as the electronic signal processing unit to reduce pick up problems. The light is thus piped from the monochromator to the detectors by means of 1 mm diameter fibers. The photocurrent pulses are treated by a computer-controlled home-

made electronic unit, which gates them, calculates their ratios square roots and averages for a fixed numbers n of shots (n=1 to 50 in practice). The code rejects shots which do not fall within 35 % of the mean reference leg. It also maintains the signal in the upper half part of the AD converter by changing electronics attenuators and PM high voltages. Moreover, it tunes the dye laser after the n shots have been collected.

For multiplex CARS, the anti-Stokes signals are dispersed by spectrographs and detected with intensified photodiode arrays (EGG 512). The dispersive element in the spectrographs is a 2100 lines/mm, aberration-corrected concave holographic grating with curvature radius of 750 mm. The spectrum is imaged with a 4× magnification optics onto the detector target. The net spectral resolution is 0.8 $cm^{-1}$ and the dispersion is 0.12 $cm^{-1}$ per diode. Both signal and reference spectra are recorded simultaneously on the signal and reference arrays and ratioed channel by channel; square roots, and averages if necessary, are subsequently processed.

*c) data processing*

For multiplex CARS, the data processing is performed by comparing the experimental profiles to the theoretical ones. Because the calculation of theoretical spectral is time consuming even with the faster computers, the use of a library of pre-calculated theoretical contours has been adopted. The different parameters like the rotational temperature, the vibrational temperature (when a nonequilibrium regime exist) are determined by using a least squares routine giving the best fit between the profiles. With this data processing, the standard deviation of the temperature remains less than 4 % for conditions of temperature and pressure equal to 3200 K and 1 bar respectively.

Scanning CARS is usually set up to analyze low density media such as hypersonic flows, discharges, low pressure CVD reactors.. As often when scanning CARS is used to analyze a low-pressure medium, the spectrum is composed of isolated lines. The logical way to process the data has been fully explained in Ref 27: The rotational temperature, the vibrational temperature and finally the density are successively inferred. The rotational temperature $T_R(V)$ of the vibrational band V is measured by plotting the natural logarithm of the lines amplitudes versus the energies of the lower states of the Raman transitions. From the expression of $\chi^{(3)}$, it can be seen that the line amplitude is proportional to the rotational population difference and so to the rotational population if one assumes that the rotational temperature does not depend on the vibrational band. The diagram is called a Boltzmann diagram. $T_R(V)$ is obtained from a linear regression with an accuracy $\Delta T_R$. $\Delta T_R$ depends on :

- the number of rotational lines and the energy gap between the lower and the upper energy levels which have been probed,
- the signal to noise ratio at peak intensity of each rotational line
- $T_R(V)$. A simple calculation shows that $\Delta T_R$ is proportional to the square of $T_R(V)$ for fixed above conditions.

As a consequence, $\Delta T_R$ ranges generally from 10-50 K for low V and increases rapidly for high V when the signal strength decreases. Furthermore, it is found that $\Delta T_R$ is in good agreement with the standard deviation of repetitive measurements.

The total population difference between the V and V+1 vibrational states are calculated assuming a Boltzmann distribution at $T_R$ on the entire vibrational bands. Each vibrational band strength is corrected for the dependence of the Raman cross section on (V+1) and the line profile through the Doppler effect.

Once the signal strength dependence have been taken into account, the vibrational population is then obtained from

$$N_V = \sum_{V'=V}^{V\,max} \Delta N_{V'} + N_{V\,max+1}$$

Where $V_{max}$ is the quantum number of the upper level of the last observed band. The population of this level may be extrapolated from the lower populations. Its value does not modify appreciably the vibrational population distribution. A Boltzmann diagram of the vibrational populations yields the vibrational temperature if existing. Summing the vibrational populations gives the total number density of the species.

Using dual-line CARS, one no longer obtains a spectrum. Supposing the $\omega_2$ and $\omega'_2$ lasers are tuned on the rotational Q-lines J and J', the electronic system delivers four signals: two signals from the reference channel R(J) and R(J'); two signals from the measuring channel S(J) and S(J'). The software calculates the ratios $Q_1$=S(J)/R(J), $Q_2$=S(J')/R(J') and $Q=Q_1/Q_2$. First, the rotational temperature $T_R$ is inferred from the following expression

$$T_R = \frac{\Delta E/k}{\frac{1}{2}LnQ + \frac{\Delta E}{kT_{ref}} - \frac{1}{2}LnA}$$

Where k is the Boltzmann constant, $\Delta E$ is the energy difference between the rotational levels J and J', $T_{ref}$ is the temperature in the reference cell and A is a constant deduced from an experiment carried out in a gas at known temperature. In the derivation of the latter expression, it is assumes that the rotational population distribution is Boltzmann-like and identical for the vibrational states coupled by the Raman transitions. Then once $T_R$ is known, the density is deduced from $Q_1$ or $Q_2$.

***d) practical applications***

While CARS has been primarily used in combustion research, work at lower pressures in plasmas, gas laser media, and aerodynamic flows has been performed. To our knowledge, the only research in practical hypersonic wind tunnels have been obtained, including frees streams and shock layers.

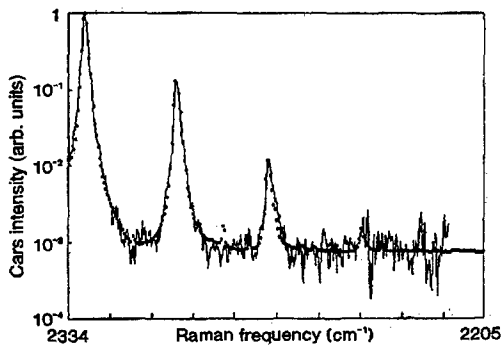


***Figure 7*** Typical single-shot multiplex coherent anti-Stokes Raman scattering (CARS) spectrum of the plume of decomposition products of a lead azide pellet 33 mm above the pellet and 9 ms after ignition

In particular, the multiplex CARS, mainly used in combustion media [24, 25] where density is relatively high, was recently used in the expanding plume of the decomposition products of lead azide, exposing a nonequilibrium gas and demonstrating, a priori, the feasibility of this technique for short-duration flows at static pressures a few $10^{-3}$ normal [26]. Figure 7 show a typical single-shot experimental spectrum of $N_2$ following the detonation of lead azide and its best fit. The theoretical spectrum is calculated for $T_R$ =200 K for all the vibrational states. The vibrational temperature of V=0 to 4 is Boltzmann-like with a vibrational temperature of 2000 K. Time sequential behavior of the $N_2$ product obtained from detonation of lead azide is also shown in Figure 8. $T_V$ decreases while $T_R$ increases as the CARS pulses is delayed. The cloud velocity is estimated to be 4000 $m.s^{-1}$. The behavior of $N_2$ is then characteristic of a product at high temperature and at high density formed near the surface of the explosive and expanding at a supersonic velocity. As a result, the rotational temperature rapidly decreases. The vibrational degree of freedom of $N_2$, remains poorly coupled to translation and rotation with a higher temperature than rotational temperature.

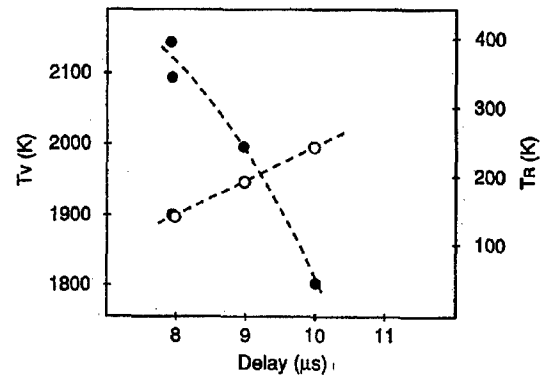


***Figure 8*** Rotational (○) and vibrational (●) temperatures evolution versus time obtained from spectra such as of Figure 7.

An illustration of the capability of the scanning CARS spectroscopy on nitrogen can be shown from the experimental study conducted in the arc driven wind tunnel L2K described previously [27]. The objective of this study was to investigate the nonequilibrium shock layer air flow induced by a two dimensional body (disk model). Preliminary measurements were carried out at a position of 555 mm downstream the nozzle exit and on the centerline region of the nozzle flow to determine the free stream conditions. Figure 9 shows a sample nitrogen CARS spectrum recorded in the free stream using the scanning CARS technique. The spectral bands detected are identified as the Q branches of the vibrational transitions (0,1) and (1,2). For each transition, clearly resolved are the rotational distributions of the two states of the molecule; the para-$N_2$ and the ortho-$N_2$ corresponding to the odd values of J and the even values of J respectively. The rotational distributions in each vibrational transition gives a rotational temperature of 330 K ± 6 K and 334 K ± 9 K for the (0,1) and (1,2) transitions respectively and demonstrates a non-dependence of the rotational distributions versus V. The vibrational temperature, measured from the ratio between V=1 and V=0 populations is 2510 K ± 130 K where the

accuracy reflects the uncertainty on the vibrational populations. A number density of nitrogen of 2.25 $10^{15}$ molecules.cm$^{-3}$ is found from the intensity of the nitrogen spectrum.

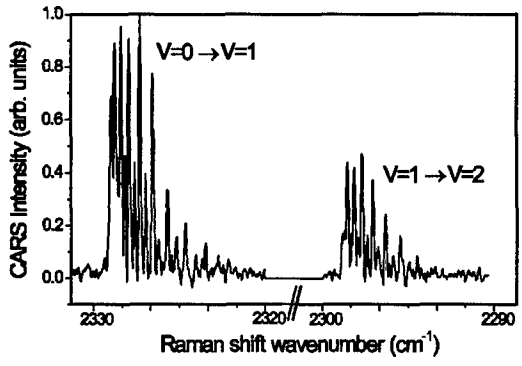


***Figure 9*** Scanning coherent anti-Stokes scattering (CARS) spectrum of $N_2$ in the free stream at the LBK wind tunnel facility.

CARS measurements are then performed between the shock layer and the model. For instance, Figure 10 shows a typical nitrogen CARS spectrum recorded at 2 mm from the model where rotational lines up to J=50 are detected in each vibrational band. As previously, rotational and vibrational temperatures and $N_2$ number density have been measured. The two resulting distributions are still found in equilibrium and the rotational temperatures associated to the two vibrational bands are equal to 4200 K ± 150 K. The vibrational temperature is found less than the rotational temperature (≈2800 K).

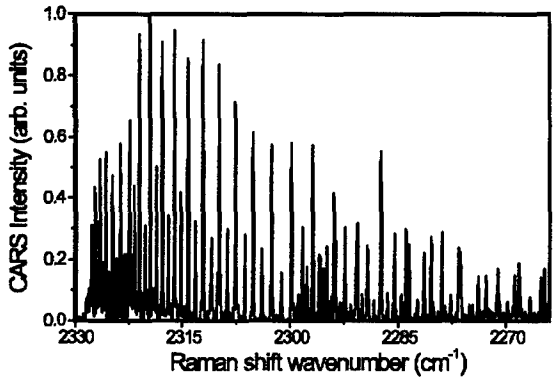


***Figure 10*** Scanning coherent anti-Stokes scattering (CARS) spectrum of $N_2$ behind the shock layer induced by a disk model.

Figure 11 shows a comparison between the experimental and theroretical temperature distributions on the symmetry axis in the shock layer. The experimental results brings into evidence the important increase of the rotational temperature through the shock wave. The rotational temperature, assumed to be also the translational temperature displays then a flat profile in a large portion of the shock layer before decreasing strongly close to the wall. On the contrary, the vibrational temperature varies slowly in the shock layer. Good agreement is achieved between these profiles and theoretical ones simulated by a Navier-Stokes solver, demonstrating the potential of this technique.

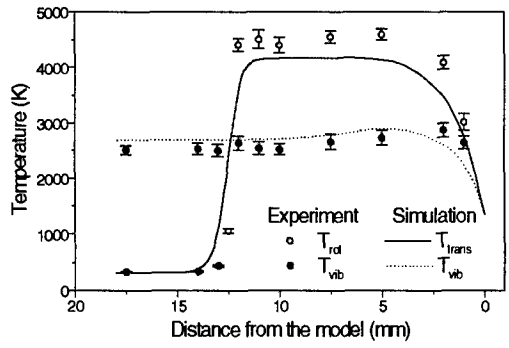


***Figure 11*** Comparison between the axial temperature distributions recorded by CARS downstream from the bow shock and the numerical predictions.

At last, dual-line CARS is shown to be well adapted to study media having low density and short run time. This is demonstrated by the spatially resolved and time-resolved rotational temperature and $N_2$ number density measurements which have been recorded in several configurations. In particular, the case of the interaction between the boundary layer and the shock wave in the vicinity of a two-dimensional compression corner has been studied [28]. The experiment was performed in the R5Ch low enthalpy blow down wind tunnel. This facility produces a Mach 10 flow for a stagnation pressure of 2.5 $10^5$ Pa. Under these conditions, the free-stream pressure, static temperature and total density are 5.9 Pa, 52.5 K and 3.9 $10^{-4}$ Kg.m$^{-3}$ respectively. Figure 12 presents the rotational temperature and density profiles measured using the dual-line CARS at five sections located between X/L=0.4 and X/L=1.2. The first two positions are located upstream of the separation line. At X/L=0.4, the temperature and the density are those of the free stream for Y=0.017 m. The temperature and the density found at Y=0.017 m are due to the shock-wave created by the leading edge interaction. For Y=0.017 m, the temperature increases through the boundary layer due to the viscous effects which decelerate the flow, and then decreases to reach the wall. Meanwhile, the density decreases and then is nearly constant in the part of the boundary layer close to the wall. At X/L=0.6, the same behavior is observed. At the

other positions, the profiles present the same features and reflect the evolution of the boundary layer along the model. The density profiles show clearly the effect of the shock induced by the ramp. For instance, the density jump observed at X/L=1.0 and located above Y=0.035 m is mainly due to the leading-edge shock and the density jump located at Y=0.026 m is due to the separation shock. As illustrated on the fig. 12, these experimental results can be used as a data bank to validate calculations performed using a Navier-Stokes solver.

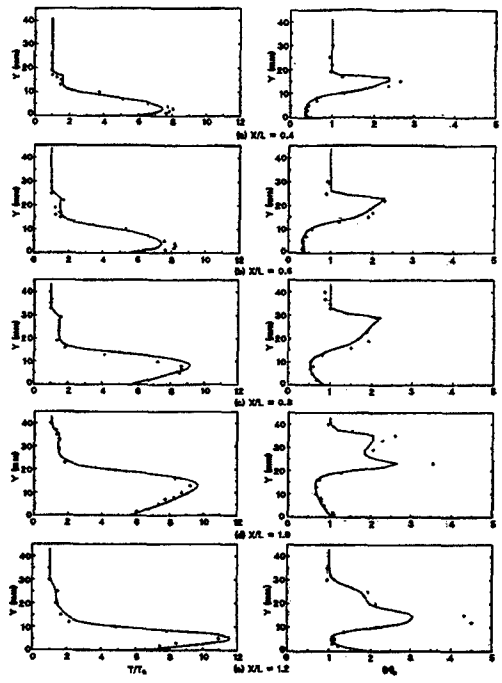

*Figure 12* Rotational temperature (left) and total density (right) distributions normalized by the free stream conditions (-)Homard2 code;(+) experiment.

## *Line-of-Sight techniques*

Line of sight methods essentially rest on emission and absorption spectroscopy.

***Emission***

In emission, one collects the light coming from the flow or from some boundary layer. This light is passed and dispersed through a spectrograph for analysis. Spectral lines are generally detected that reveal the presence of chemicals like metal vapors (in the visible or ultraviolet) or of vibrationally excited molecules. Presence of these lines indicates presence of the compound. The method suffers from major drawbacks, such as the impossibility of determining the position of the radiating species along the line of sight of the collection optics; this is fatal if zones of different temperature and concentration is contributing. In addition, it is also impossible to determine temperature concentrations in a quantitative manner, even if only a homogeneous zone contributes. The latter difficulty stems from the fact that the radiating quantum states are populated via complex collisional mechanisms with electrons or hot species in the nonequilibrium flow and are depopulated by both radiative and collisional (quenching) processes with other species. Emission is this primarily for establishing the presence of trace species or contaminants.

***Absorption***

Absorption techniques are capable of measuring populations of the ground rovibrational states, which are the most populated. Therefore, concentrations can be measured (at least if the absorbing medium is homogenous or presents some spatial symmetry). Technically, the best measurements are performed with laser tunable sources having a spectral resolution capable of resolving the molecular or atomic lines. Currently, the diode laser absorption spectroscopy (DLAS) technique in the infrared is attractive to perform measurements in a wide variety of aerodynamic flows [29, 30, 31]. Measurements in hypersonic flows are usually performed on heteronuclear molecules like CO, NO and $H_2O$ which have strong absorption line strengths due to their high dipole moments. The fundamental level absorption lines for these molecules are usually in the mid infrared region (wavelength > 4 μm).

***a) Principle***

The technique is based on semiconductor diode lasers which are well adapted to absorption spectroscopy. These lasers have very narrow line width emissions (a few tens of MHz) which can be tuned precisely (with a resolution close to $10^{-4}$ $cm^{-1}$ ) around absorption lines, allowing one to visualize the temperature and pressure broadening without any disturbance broadening from the laser linewidth itself. Therefore, this high spectral resolution feature allows linewidth measurements of temperature and concentrations of trace molecules in low pressure (less than 1000 Pa) chemically reacting media such as in hypersonic flows where the lines are mainly broadened by temperature effects with typical Doppler line widths of $10^{-2}$ $cm^{-1}$. The gas velocity can also be determined from the Doppler shift induced in the line positions of the absorbing species when the beam is not perpendicular to the flow axis. The Doppler shift is on the order of $10^{-2}$ $cm^{-1}$ at 5 μm for bulk velocities above 1000 m/s. The allowed measurements are illustrated in Figure 13 from a spectrum presenting an NO absorption line with its Doppler-shifted component. The unshifted line results from absorption of molecules at low velocities which are in the boundary layer of the flow or outside the

flow. For $H_2O$, there is also a contribution from the ambient humidity of air outside the test section.

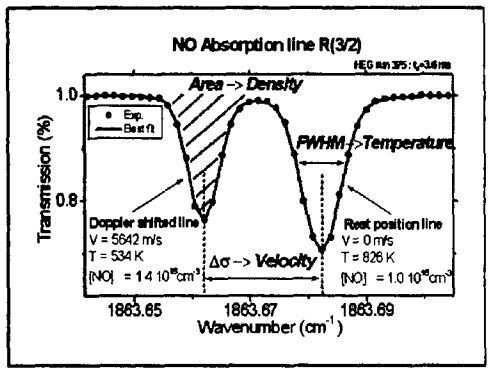


*Figure 13* Usual parameters which can be deduced from pressure-free absorption lines

A major disadvantage of this technique is its line-of-sight nature which gives integrated or averaged data over the absorption path through the medium crossed. The Doppler shifting helps to discern the flow core properties from other zones with molecules absorbing at lower velocities. Another drawback of the technique, carried out in the mid infrared (>2.5 μm), is the requirement to use cryogenic technology: liquid nitrogen cooling for both the diode laser (working around 100 K) and HgCdTe detectors. The main advantages are its sensitivity and its capability to perform measurements at relatively high frequency. Spectra recording can be repeated up to several tens of kHz, which is a very attractive feature for high enthalpy blow-down facilities where the flow runs for short periods (about 200 ms for arc-driven facilities like F4), and where the thermodynamic parameters change over characteristic times of about 10 μs to 1 ms.

***b) Experimental setup***

The laser emission bench and detection setup has been described in detail elsewhere [32]. It can be equipped with two diodes working at temperatures around 100 K. Usually, these diodes emit only over allowed modes covering spectral windows about 1 $cm^{-1}$ wide. With proper tuning of the temperature and current of the diode, some of the spectral windows can be made to come into coincidence with absorption lines of the molecules to be probed. Out of these, only a few lines showing absorption above the detection limit and below saturation can be used, after proper evaluation from the expected densities and temperature of the flow to be probed. A typical emission mode covering some NO absorption lines is presented in Figure 14. This "1864 $cm^{-1}$" mode is the most widely used to probe NO or $H_2O$ in F4 because of the absorption lines contained in it allowing a probe of nearly all the flow conditions. A few hundred sets of flow absorption spectra are acquired together with their corresponding calibration spectra, during each run. Each spectrum is sampled with 1000 spectral points spaced at less than $10^{-3}$ $cm^{-1}$, so that a pressure-free FWHM line profile, which is typically $10^{-2}$ $cm^{-1}$ wide, is described by about 20 spectral points. After wavelength and intensity calibration with the help of the calibration channels, the useful segment of each corrected spectrum is matched to simulated spectra through an iterative non-linear least-squares fitting procedure [32] to retrieve the velocity, the kinetic temperature, and the concentrations of the absorbing species.

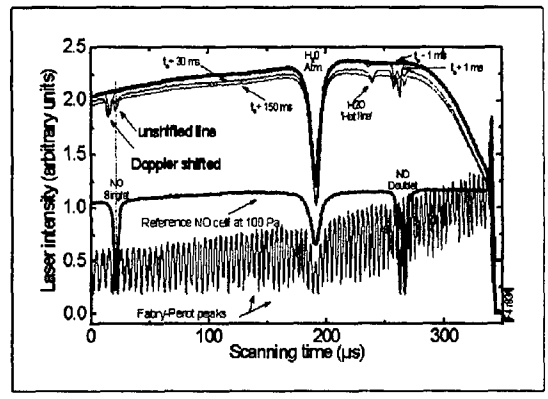


*Figure 14* Typical flow absorption spectrum together with associated calibration spectra

A simple two-layer model is assumed for the flow to perform the data reduction [32]. One layer corresponds to the core flow with a constant free stream velocity v and is usually called the Doppler layer. The other layer (called external or 'rest position' layer) includes all the gases outside the flow core with no bulk velocity that contribute to rest-position lines in the absorption spectrum. This model has been justified experimentally by the use of pipes to protect absorption of the laser beam through the boundary layer (see sections 3 and 4 below) : the comparison of the absorption with and without pipes show that molecules with intermediary velocities in the boundary layer contribute very little to the absorption spectra. Thus, the Doppler shifted and the unshifted line corresponds to only two zones : respectively, the flow core at high velocity and the region outside the flow at thermal velocity.

***c) practical applications***

We present here some applications in the F4 wind tunnel generating high enthalpy flows where molecules like CO, NO, $H_2O$ are naturally present as a result of real gas effects or trace pollution species. Measurements on $H_2O$ in a low enthalpy hypersonic wind tunnel (S4MA) is also presented to illustrate the wide range of application of this technique. Figure 1

summarizes the principal reservoir characteristics and the flow duration times of the wind tunnels probed. The F4 arc-driven, hot-shot, high enthalpy facility was built to simulate part of the re-entry trajectory of space vehicles in the upper atmosphere. It has been extensively described elsewhere [33, 34].

The S4MA facility is a cold blow-down hypersonic wind tunnel operating at Mach numbers of 6.4, 10 or 12 [35]. For reentry studies, it is a common use to obtain reference points where there are no real gas effects. In order to avoid liquefaction, the stagnation conditions (up to 15 MPa for pressure and up to 1800K for temperature) are obtained by passing compressed air in an accumulation heater containing 11 tons of alumina pebbles heated by propane combustion before a run. The run can last up to 100 s, but usually the first 10 to 25 s are used to stabilize all flow parameters at the expected values. This stabilization time is suspected to be due to air liquefaction and water vapor condensation at the beginning of the run.

• *F4 experiments*

The laser beam from the emission bench enters the vacuum chamber through $CaF_2$ windows and crosses the flow at the smallest possible angle to the flow axis (around 63°, given the distance between nozzle and diffuser ) so as to induce the largest Doppler shift for velocity measurements. The portion of the flow which is probed is roughly a cylindrical volume of about 670 mm in diameter (nozzle n° 2 exit diameter with a 400 mm diameter flow core) over a path length of about 400 mm.

The laser beam was guided through profiled sealed pipes to avoid the absorption contribution from lower velocity and higher temperature molecules in the flow boundary layer which can disturb the absorption line shapes in the flow core. The tube ends generate a boundary layer of their own, but its contribution to the absorption lines was assumed to be negligible as it does not exceed a thickness of a few millimeters. It was too difficult to have such sealed pipes on the whole path of the laser beam inside the test section because of the mirrors used to obtain the necessary angle of the beam with respect to flow axis for the Doppler-shift velocity measurements. Nevertheless, this configuration reduced the absorbing molecules to only two groups : molecules of the flow core at bulk velocity of the flow giving the Doppler shifted lines and molecules only at thermal velocities giving the unshifted absorption lines. The data reduction is therefore easier and justifies completely the two layer model mentioned in section 2 above. In fact, comparisons of results for similar runs with and without protection pipes shows that the protection pipes only bring a decrease in the intensity of the non-shifted absorption lines, but little or no difference for velocity and temperature measurements, confirming that boundary layers have indeed little impact on the measurements [36].

The flow can last up to 400 ms, with its thermodynamic parameters rapidly changing as the gas is expelled out of the arc chamber (about 1%/ms decrease of total pressure and enthalpy). The spectra acquisition is therefore set in this facility to 1 kHz for a total measurement time of 1 second. Usually, the data reduction on the absorption spectra is performed for the first 120 ms of the run, because the Doppler shifted absorption line in the flow becomes too small or the results to be reliable after this period.

The typical values of free stream velocity, temperature and NO density versus time for a type III flow using nozzle n°2 are shown in Figure 15. These values are also compared to results obtained from several numerical flow models [37]. The velocities inferred from the spectra are lower than the values calculated from heat flux measurements using frozen and equilibrium flow assumptions in the first 40 ms but the theoretical/experimental agreement is good after 40 ms. Note that the first 30-40 ms of F4 runs are considered as a flow establishment period due to the nozzle plug and wires expelling phase. The other gas parameters do not compare well: the DLAS temperature is higher even than the equilibrium one, whereas the NO density is lower than the frozen one. Some attempts to explain these discrepancies are described in ref. 37.

Experiments are carried out with a diode laser tuned on a CO absorption line (the R8 line at 2176.2835 $cm^{-1}$). Figure 16 shows the corresponding results of free stream velocity, temperature and CO density for a run having a lower enthalpy condition than for a type III condition. These results are still being analyzed and will be published shortly. The CO is presently believed to result, first, from organic material (seals, silicon paste...) ablation with pure nitrogen runs, second, from combustion processes taking place in the arc chamber where the temperature is very high (up to 8000 K) and where the thermal protection elements are mostly in carbon materials. Further tests with nitrogen will allow to quantify these two contributions.

The least-squares fit, using the two-layer model, gives uncertainties of about 1% for velocity and 10% for both temperature and density. We must add to this, uncertainties from spectrum calibration and setup configuration (for example the angle of the laser beam to the flow axis is known with only 1 degree accuracy resulting in an uncertainty of 4% on velocity). The overall uncertainties are then estimated, for both

probed molecules, to be less than 10% for velocity and 30% for both temperature and density.

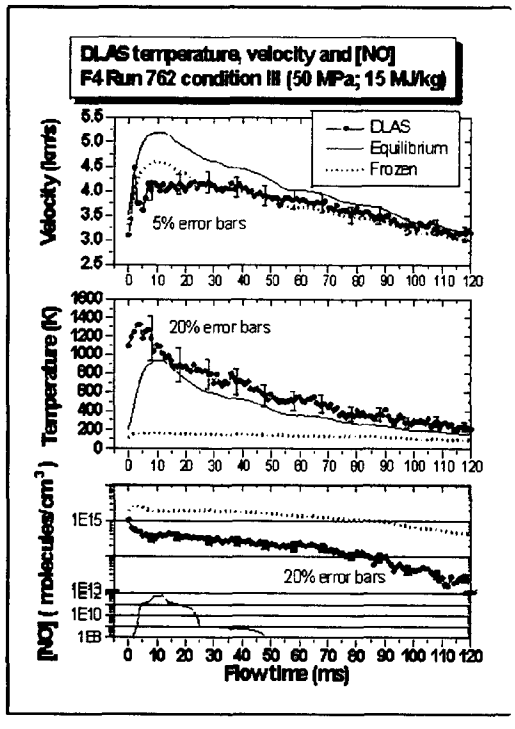


*Figure 15* Velocity, translational temperature and NO density from DLAS in F4 air run.

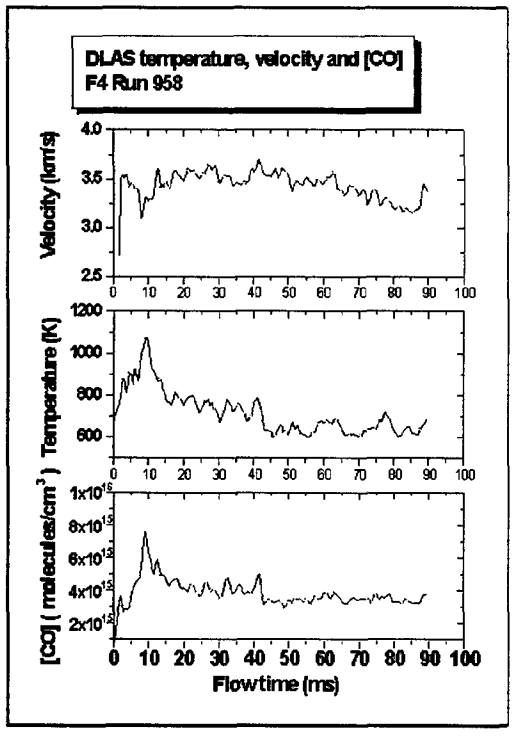


*Figure 16* Velocity, translational temperature and CO density from DLAS in F4 air run.

• *S4MA experiments*

The aim of the diode laser measurements was to measure the water vapor in the flow so as to see the impact of its concentration on the stagnation conditions stabilization time encountered in this wind tunnel.

The laser diode used here has been specifically chosen to emit in a spectral window covering two of the most intense absorption lines of $H_2O$ (1616,1135 $cm^{-1}$ and 1653.2671 $cm^{-1}$ ). This was required to measure the quite low water vapor density expected in the free stream : about $10^{12}$ molecules/$cm^3$, which makes about 13 ppm in the free stream of total mass density of 0.01 kg/$m^3$ and at the temperature of 50K. One of the main problems in the experimental setup is to avoid saturation of the absorption line from ambient water vapor and from the low pressure contribution in the test section outside the flow.

These feasibility experiments were done with the laser beam crossing perpendicularly to the flow in order to check if the signal-to-noise ratio is sufficient to obtain measurements. This of course denies the possibility of velocity measurements as there is no Doppler shift in the absorption lines.

The probed zone was a cylinder of diameter 8 mm and of length ranging from 0,6 meter (flow core only) to 1 meter (flow core and boundary layer). The rest of the laser path is protected in tubes (of variable length) flushed with dry nitrogen in order to avoid absorption by low pressure water vapor absorption outside the flow or in the boundary layer. The emission and detection benches are also flushed with dry nitrogen to avoid absorption from atmospheric water vapor outside the test section.

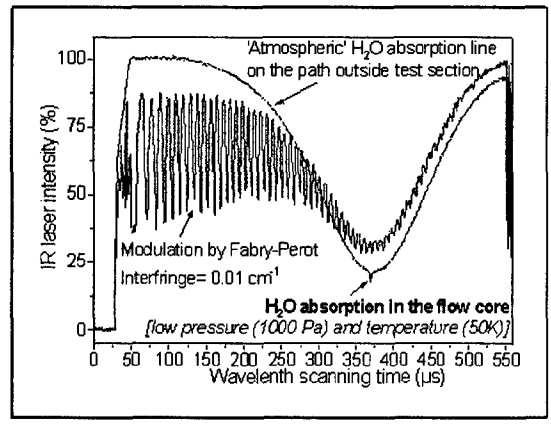


*Figure 17* Typical flow absorption spectrum recorded together with associated calibration spectra

The unwanted absorption from outside the test section was the most difficult to eliminate : the $N_2$ flushing only reduced this saturated absorption to an 80-90% absorption. Fortunately, this was enough to allow us to see the small absorption (a few %) of the water vapor in the flow. The width of this absorption line is narrower (because of the low pressure and low temperature) than the atmospheric $H_2O$ line. The absorption spectrum in Figure 17 illustrates this difference in the line widths. As the atmospheric $H_2O$ absorption line can be considered to be constant during the flow time of 100 seconds, it was also considered as a mere emission envelope during the data reduction.

Spectra were acquired every 0.1 seconds for a total time of 100 seconds which was more than enough to cover the total flow time set to about 60 seconds for these experiments. After calibration and inversion, the time evolution of water vapor density in the flow can be traced as illustrated in Figure 18 where three runs at three different reservoir temperatures (nominal values of 980, 1030 and 1120 K for runs R3063, R3064 and R3065 respectively) are compared. These density curves are also compared to the Mach number and temperature temporal evolution of the flows considered. It was not possible to measure the water vapor density for very low temperatures as the absorption line was below the detection limit of our instrument. The curves in Figure 18 show that there is a threshold temperature (~46K) above which the absorption line could be detected.

These results show that the water vapor content in the free stream is very low as expected. Its density increases with flow time and has the same temporal trend as for Mach number or temperature. A possible explanation is that at the beginning of the run, the water is not only in vapor form, but also in liquid and solid form; after the first seconds of the run, as the temperature increases, the increase of water vapor content can indicate a decrease of the water vapor condensation, and appears to be a positive sign for good flow parameters. Also, there can be other reasons for the stagnation conditions stabilization time, like air liquefaction, or dust due to ablation of the heating pebbles coming mostly at the beginning of the flow. Other types of experiments are now being planned to measure water in form of solid or liquid as well as to measure dust particles which can enhance air liquefaction at the beginning of the blow down.

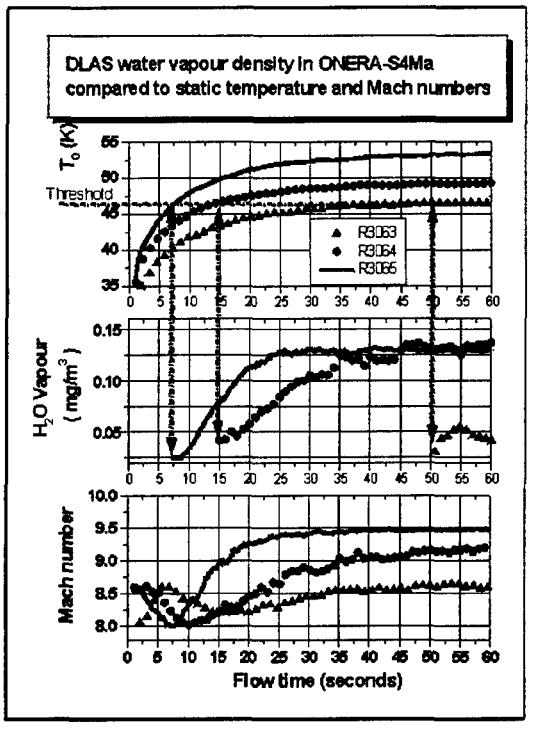


*Figure 18* Time evolution of the temperature, water vapor density and Mach number during three runs at S4MA.

## Conclusion

With the new laser sources now available, there are numerous approaches to acquisition of the flow parameters for probing hypersonic flows in ground testing facilities.

In high-enthalpy facilities, diode laser absorption spectroscopy is well suited for free stream measurement of velocity, static temperature and trace species concentration measurements. However, it requires the flow to be quite homogeneous. CARS is a good tool for point measurement of rotational and vibrational temperatures and of number density. Electron beam fluorescence and Laser Induced fluorescence can be employed for qualitative imaging and visualization. Visualization of shocks and in particular the convection of a plasma column can be used to measured the velocity profiles.

In low-enthalpy flows, the same methods can be also employed. However, if density is higher, Diode laser absorption will lose ground in the velocity measurements and seeding with NO or other species may become necessary. EBF will also lose all of its applications, while the optical techniques like Rayleigh and Raman scattering will become applicable.

**Acknowledgments**
I am indebted to the many members of the ONERA research group who have contributed to the research described in this article. In particular, I am grateful to A. Mohamed and S. Larigaldie for permission to cite aspects of their research works. I am grateful also to U. Koch and A. Gülhan from DLR for permission of their results and J.P. Taran from Onera for helpful discussions.

## References

[1] Boutier A., "News trends in Instrumentation for hypersonic research". Proc. NATA Adv. Res. Workshop Instrum. Hypersonic Res., ONERA Le Fauga-Mauzac Center, France, Series E: Applied Sciences, Vol 224, 1992.

[2] "Aerodynamic measurement technologies", AIAA J, 34 (3), pp 433-526 ,1996.

[3] Miles R.B., Lempert W.R., "Quantitative flow visualization in unseeded flows", Ann. Rev. Fluid. Mech. 29, pp 285-326, 1997.

[4] Byer R.L., "Review, remote air pollution measurement", Opt. Quant. Elect. 7, pp 147-177, 1975.

[5] Bobin L., "Experimental investigation of a jet in a cross flow by spontaneous Raman scattering", ICIASF, ISL, Saint Louis, France, EEE Publ. 93CH3199-7, 1993.

[6] Gillepsie W.D., Bershader D., Sharma S.P., Ruffin S.M., "Raman scattering measurements of vibrational and rotational distributions in expanding nitrogen", AIAA paper 93-0274, 1993.

[7] Palmer J.L., McMillin B.K., Hanson R.K., "Planar Laser-Induced fluorescence Imaging of velocity and temperature in Shock tunnel free jet flow", AIAA 92-0762, 1992.

[8] Hanson R.K., "Combustion diagnostics: Planar Flowfield Imaging" twenty First Symposium (International) on Combustion, The Combustion Institute, pp 1677-1691, 1986.

[9] Kychakoff G., Howe R.D., Hanson R.K., "Use of Planar Laser Induced Fluorescence for the study of Combustion Flowfields", AIAA paper 83-1361, 1983.

[10] Lucht R.P., "Laser Spectroscopy and its applications", Eds. L.J. Radziemski, Solanz R.W., Paisner J.A., Marcel Dekker, New York, pp 623-676, 1986.

[11] Bechtel, J.H., Dasch, C.J., Teets R.E., Laser Applications, Academic Press, New York, 1984.

[12] Cattolica R.J., Vosen S.R., Twentieth Symposium (International) on Combustion, The Combustion Institute, pp 1273, 1985.

[13] Seitzman J.M. , Hanson R.K., "Quantitative Fluorescence Imaging: A Comparison of Linear, Predissociative and Saturated Pumping Techniques", AIAA paper 92-0879, 1992.

[14] Marinelli W.J., Kessler W.J., Allen M.G., Davis S.J., Arepalli S., Scott C.D., "Copper atom based measurements of velocity and turbulence in arc jet flows" AIAA paper 91-0358, 1991.

[15] Bamford D.J., O'Keefe A., Babikian D.S., Stewart D., Strawa A.W., "Characterization of arc-jet flows using laser-induced fluorescence", AIAA paper 94-0690, 1994

[16] Meyer S., Sharma S., Bershader D., Whiting E., Exberger R., Gilmore J., "Absorption line shape measurement of atomic oxygen at 130 nm using a Raman-shifted excimer laser", AIAA paper 91-0358, 1991.

[17] Koch U., Gülhan A., Esser B., Grisch F., Bouchardy P., "Rotational and Vibrational temperature and density measurements by planar laser induced NO-fluorescence spectroscopy in a nonequilibrium high enthalpy flow", RTO/AGARD fluid dynamics panel symposium, Advanced aerodynamic measurement technology, Seattle, USA, 22-25 September 1997.

[18] Mohamed A.K., Pot. T., Chanetz B., "Diagnostics by electron beam fluorescence in hypersonics", Int. Congr. Aerosp. Sim. Facil., 16 th, Dayton, OH, 1995.

[19] Lufty F.M., Muntz E.P., "Initial experimental study of pulsed electron beam florescence", AIAA J., 34, pp 478-482, 1996.

[20] Voronel E.S, Kuznetsov L.I., Parfenov M.V., Yarygin V.N., "Electron X ray method for measuring the local density in pulsed erosion jets", Quantum Electron., 24, pp 1010, 1994.

[21] Larigaldie S., Bize D., Mohamed A.K., Ory M., Soutadé J., Taran J.P., "Velocity measurement in hypersonic flows using electron beam-assisted glow discharge", AIAA J., 36, pp1061-1064, 1998.

[22] Maker P.D., Terhune R.W., "Study of optical effects due to an induced third order polarization in the electric field strength", Phys. Rev., 137A, pp 801-818, 1965.

[23] Greenhalgh, D.A., "Comments on the use of BOXCARS for gas-phase CARS spectroscopy", J. Raman Spectrosc., 14, 150-153, 1983.

[24] Eckbreth, A.C., Dobbs G.M., Stufflebeam, J.H., Tellex P.A., "CARS temperature and species measurements in augmented jet engine exhausts", Appl. Opt., 23, pp 1328-1338, 1984.

[25] Magre, P., Moreau P., Collin G., Borghi, R., Péalat M., "Further studies by CARS of premixed turbulent combustion", Combustion and flame, 71, 147-153, 1988.

[26] Rosenwaks T., Arusi-Parpar T., Bar I., Bouchardy P., Cohen Y., David D., Grisch F., Heflinger D., Péalat M., Strugano A., Taran J.P., Valentini J.J.,"Application of stimulated Raman excitation and Coherent anti Stokes Raman spectroscopy to Molecular dynamics and Gas dynamics", Nonlinear Optics, 5, pp33-44, 1993.

[27] Grisch F., Bouchardy P., Koch U., Gülhan A., Esser B., "Rotational and Vibrational temperature and density measurements by coherent anti-Stokes Raman spectroscopy in a nonequilibrium shock layer flow", RTO/AGARD fluid dynamics panel symposium, Advanced aerodynamic measurement technology, Seattle, USA, 22-25 September 1997.

[28] Grisch F., Bouchardy P., Péalat M., Chanetz B., Pot T., Coët M.C., "Rotational temperature and density measurements in a hypersonic flow by Dual-Line CARS", Appl. Phys. B., 56, pp 14-20, 1993.

[29] Arroyo M. P., Langlois S., Hanson R. K., "Diode laser absorption technique for simultaneous measurements of multiple gas dynamic parameters in high speed flows containing water vapor", Appl. Opt., vol 33, n°15,1994.

[30] Mohamed A. K., Rosier B., Henry D., Louvet Y., Varghese P. L., "Tunable diode laser measurements on nitric oxide in a hypersonic wind-tunnel", AIAA Paper 95-0428, 1995.

[31] Upschulte B. L., Miller M. F., Allen M.G., Jackson K., Gruber M., Mathur T., "Continuous water vapor mass flux and temperature measurements in a model scramjet combustor using a diode laser sensor", AIAA paper 0518, 1999.

[32] Mohamed A. K., "MSTP Phase 2 Progress Report. Infrared Diode Laser Absorption Spectroscopy in Wind Tunnels. I-Experimental Setup, II-Data Reduction Procedures" (ESA -HT-TN-E34-701&702&703-ONERA),ONERA Technical Report n° 8 and 9 /7301 PY, 1996.

[33] François G., Ledy J.P., Masson A., "ONERA high enthalpy wind-tunnel F4", 82nd Meeting of the Supersonic Tunnel Association, Wright Patterson AFB, Ohio, Oct. 16-18, 1994

[34] Vardavas I..M., "Modeling reactive gas flows within shock tunnels", Australian J. Chem., 37, pp157-177, 1984.

[35] Ledy J.P., Prieur J., "Improvement of the ONERA hypersonic facility S4MA exhaust at the atmosphere at M = 6.4", 89th Supersonic Tunnel Association International Meeting (VKI), Brussels, 26-28 April 1998.

[36] Mohamed A. K. , Rosier B., Sagnier P., Henry D., Louvet Y., Bize D., "Application of Infrared Diode Laser Absorption Spectroscopy to the F4 High Enthalpy Wind Tunnel", Aerospace Science and Technology, 4, pp 241-250, 1998.

[37] Sagnier Ph., Vérant J. L., "Flow characterization in the ONERA F4 high enthalpy wind tunnel", AIAA J., 36, pp 522-531, 1998.